OPEN ACCESS
IOP Publishing
Semiconductor Science and Technology
Semicond. Sci. Technol. **38** (2023) 055017 (13pp)
https://doi.org/10.1088/1361-6641/acc08d

Ballistic transport and surface scattering in (In,Ga)As-InP heterostructure narrow channels

A Aleksandrova[1,2,*], Christian Golz[1,2], H Weidlich[1], Mykhaylo Semtsiv[2], W T Masselink[2] and Y Takagaki[3]

[1] Institute Kurz GmbH, Stöckheimer Weg 1, 50829 Cologne, Germany
[2] Department of Physics, Humboldt University Berlin, Newton Str. 15, 12489 Berlin, Germany
[3] Paul Drude Institute for Solid State Electronics, Hausvogteiplatz 5-7, 10117 Berlin, Germany

E-mail: anna_a@physik.hu-berlin.de

Received 5 December 2022, revised 3 February 2023
Accepted for publication 2 March 2023
Published 3 April 2023

Abstract

Narrow conduction channels are fabricated from an $In_{0.75}Ga_{0.25}As$-InP heterostructure using electron-beam lithography and dry etching. The etched surface is realized to be smooth by employing a reactive ion etching. The etching-induced surface conduction is eliminated by removing the damaged surface layer using a diluted HCl solution. The negligible surface depletion for the In-rich quantum well enables to create conducting channels in arbitrary geometries such as in a circular shape. We evidence the presence of a ballistic contribution in the electron transport by demonstrating a rectification of *rf* excitations that is achieved by the magnetic-field-tuned transmission asymmetry in the circularly-shaped channels. The absence of the surface depletion is shown to cause, on the other hand, a surface scattering for the electrons confined in the channels. An increase of the resistance, including its anomalous enhancement at low temperatures, is induced by the gas molecules attached to the sidewalls of the channels. We also report a large persistent photoconduction, which occurs as a parallel conduction in the undoped InP barrier layer.

Keywords: ballistic transport, surface scattering, (In,Ga)As-InP heterostructure, narrow channel, magnetorectification

(Some figures may appear in colour only in the online journal)

1. Introduction

In circular-shaped narrow ballistic channels of a two-dimensional electron gas (2DEG), the transport becomes asymmetric with respect to the reversal of a magnetic field applied perpendicular to the 2DEG [1]. A simplified explanation of the transmission asymmetry is as follows. When the cyclotron radius r_c of the 2DEG coincides with the curvature radius R of the circular channel, the electrons rarely experience scattering from the channel boundary due to the fit of the cyclotron orbit within the channel. On the other hand, when the magnetic field direction is reversed, or equivalently for the electrons moving in the opposite direction along the circular channel, the boundary scattering is frequent since the Lorenz force pushes the electrons in the direction opposite to the curving of the channel. The transmission, therefore, becomes asymmetric when the nonspecular component of the boundary reflection causes backscattering [2]. It needs to be pointed out, however, that the transmission in two-terminal

* Author to whom any correspondence should be addressed.

geometries is well-known to be symmetric with respect to the magnetic field reversal in equilibrium [3, 4]. The transmission asymmetry has been shown to emerge by a fully quantum-mechanical tight-binding simulation when electron-electron interactions are taken into account as the on-site repulsion in a nonequilibrium transport [5].

The transport asymmetry gives rise to a rectification effect, where a DC voltage is produced from the *rf* excitation applied to the channel [1, 5]. The rectification was highly efficient to the extent that the environmental *rf* noises were rectified [1]. That is, a DC voltage was present between the two ends of the circular channel even in the absence of an intentional *rf* excitation for temperatures below 90 K. The devices can be utilized to harvest energy from environmental electromagnetic noises [6, 7]. If the energy harvesting is to be done using conventional rectifier devices such as diodes, the threshold voltage for nonlinearity needs to be lowered to the magnitude of the *rf* noises. Currently, the efficiency is about 20% for an *rf* power of 1 μW and almost zero when the *rf* power is merely 0.1 μW [8].

For the application for energy harvesting [9–12], it is desirable to raise the operation temperature of the rectification to room temperature (RT). The experiments in [1, 5] were carried out using GaAs-(Al,Ga)As heterostructures. The high mobility of the 2DEG in the GaAs-(Al,Ga)As heterostructures is ideal to demonstrate the ballistic transport effect at low temperatures. The electron mobility, however, decreases with increasing temperature due to the scattering by phonons. For raising the operation temperature, the devices need to be made smaller to overcome the reduction of the mean free path l_e. Here, narrow channels fabricated from the GaAs-(Al,Ga)As heterostructures exhibit a large sidewall depletion, which is problematic for the curved geometry to reduce the size of the narrow channels. An attempt was made, therefore, to produce the curved channel using (In,Ga)As-InP heterostructures [13]. The negligible surface depletion for the (In,Ga)As-based heterostructures allows us to reduce the curvature radius of the circular channel to be as small as limited by the lithography and etching techniques. The use of (In,Ga)As-InP heterostructures has another advantage for the RT operation of the ballistic transport devices. Although the low-temperature mobility in (In,Ga)As-based heterostructures is not competitive in comparison to the high mobility in GaAs-(Al,Ga)As heterostructures due to the alloy scattering, the mobility of the 2DEG at RT is higher in the (In,Ga)As-based heterostructures in comparison to that in the GaAs-based heterostructures. In figure 1, we show the temperature dependence of the mobility μ obtained from a number of $In_{0.75}Ga_{0.25}As$-InP heterostructures. The mobility at RT is limited by the scattering from polar optical phonons. The RT electron mobility in the $In_{0.75}Ga_{0.25}As$-based heterostructures is higher than that in the GaAs-(Al,Ga)As heterostructures primarily reflecting the effective mass of 0.032 and 0.063 of the electrons in the respective heterostructures. By optimizing the design of the heterostructures, the mobility can be larger than 1 $m^2\,V^{-1}\,s^{-1}$ at RT.

In [13], (In,Ga)As quantum wells grown on InP substrates were etched using Ar ion milling to fabricate narrow channels. The Ar ion milling was found to roughen the surface of the heterostructures as well as the InP substrates significantly. The etching method is thus unsuitable to fabricate narrow channels from the materials containing In. There are reports on self-organized structuring in the etched surface of InP in the form of small globules, nanopyramids, and nanowires [14–16]. Dry-etching methods are one of the key technologies for achieving high geometrical accuracy and uniformity in the device production in the full wafer size [17, 18]. The method is used in producing optoelectronic devices because of its high resolution, good reproducibility, and easy control of process conditions [16]. To fulfill the need to obtain smooth surfaces for the industrial applications, reactive ion etching of In-containing surfaces has been investigated [19, 20].

In this paper, we accomplish to realize smooth etched surfaces in the fabrication of narrow channels from an (In,Ga)As quantum well structure using a reactive ion etching. The sidewall depletion in the channels is demonstrated to the negligible. The transport properties in circular-shaped narrow channels are investigated in the presence of a magnetic field to establish the existence of contributions from the ballistic transport of electrons. We additionally show a surface scattering in the channels caused by external environmental effects. The influences of the persistent photoconduction in the undoped InP barrier layers on the transport properties are furthermore presented.

2. Fabrication of narrow channels

The epitaxial growth of the (In,Ga)As quantum-well structure was carried out in a Riber Compact 21 T gas-source molecular-beam-epitaxy (GS MBE) system. Solid sources were used for In, Ga and Al, while As and P were supplied as pre-cracked arsine and phosphine, respectively. The heterostructure consisted of a 13 nm thick $In_{0.75}Ga_{0.25}As$ layer sandwiched between a 44 nm thick InP capping layer and the InP buffer layer grown on a (100)-oriented semiinsulating InP:Fe substrate. The heterostructure was undoped. The conduction electrons were supplied to the (In,Ga)As quantum well from crystalline defects, which acted as donors. For the similar reason, the InP buffer layer was slightly conductive. This required the buffer layer to be removed completely in fabricating narrow channels. The buffer layer was thus chosen to be thin (14 nm thick). The samples shown in figure 1 were grown using the same GS MBE system. Although the system is capable of achieving a mobility of 7 $m^2\,V^{-1}\,s^{-1}$ at low temperatures, the mobility of the 2DEG employed in this work suffered to be relatively low due to the scattering from the Fe dopants in the InP substrate.

The narrow channels were defined using electron-beam lithography. Patterns made of a Ti layer were prepared using the lift-off technique on the surface of the (In,Ga)As-InP heterostructure to be used as the mask in the subsequent dry etching. A reactive ion-beam etching was carried out at the Heinrich Hertz Institute [21] to transfer the mask pattern to the underlying heterostructure. The depth of the etching was

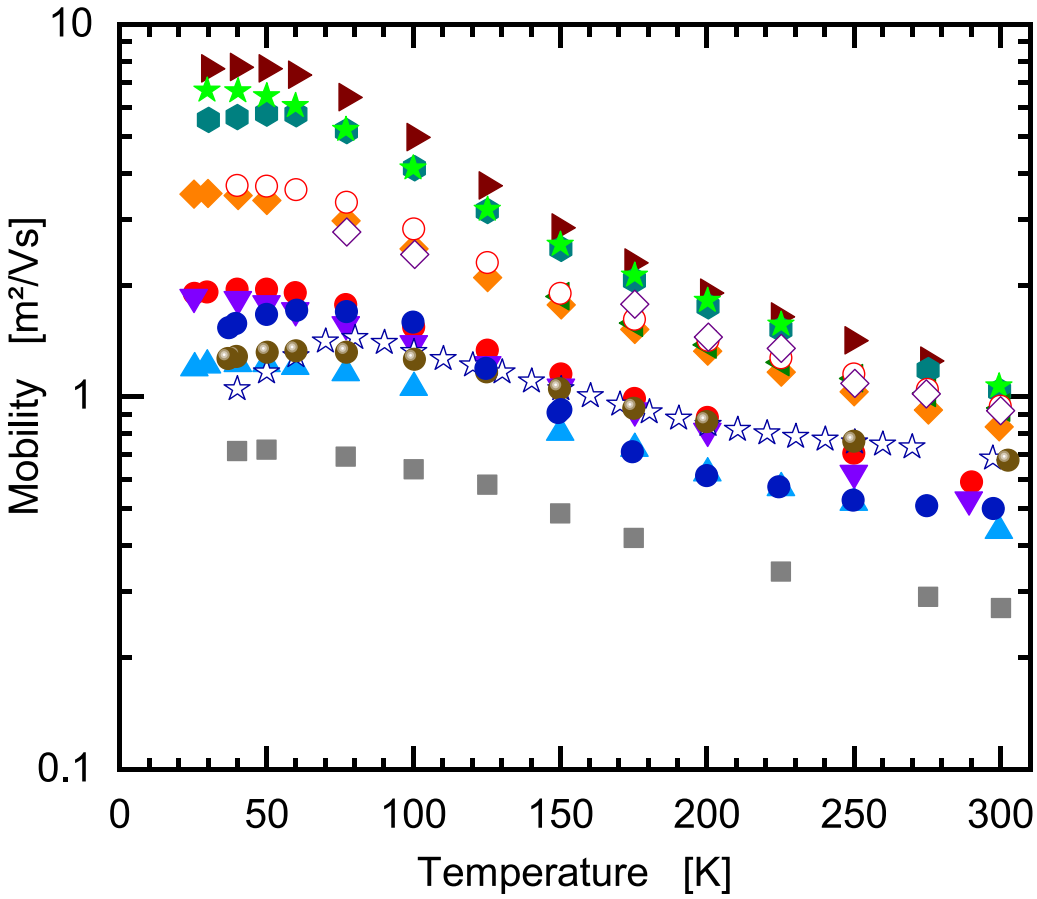

Figure 1. Mobility of two-dimensional electron gases in $In_{0.75}Ga_{0.25}As$-InP heterostructures. The temperature dependence is compared for the heterostructures grown by a GS MBE system. The thickness of the InP-buffer layer and the density of Si doping were changed in the heterostructures. The open and filled symbols correspond to undoped and doped structures, respectively. The sheet electron concentration at low temperatures was in the range of $5 \sim 11 \times 10^{15}$ m^{-2}.

190 nm. In figure 2, we show scanning electron micrographs of the channels prepared in the heterostructure. The etched surface is seen to be smooth. The smoothness enabled us to fabricate narrow channels, as shown in figure 2(b). Here, the width of the curved part of the channel is 90 nm, as one finds in the expanded image.

In the previous study of the nanostructuring in [13], the narrow channels were fabricated using Ar ion milling. In addition to the roughening of the etched surface, another problem arose there from the fact that the crystalline defects induced by the Ar sputtering generated carriers. The etched surface consequently became conductive. Although the etched surface has been improved to be smooth using the reactive ion etching in the present work, the surface conduction still persisted. The etching induced surface conduction is a common feature in the dry etching of In-containing surfaces regardless of the smoothness of the surface. Various methods have been reported to eliminate the surface conduction. Upon annealing the etched samples at 650 °C in the atmosphere of P, removal of damages with improved surface morphology has been reported [22]. One of the possible reasons for the decrease in the surface resistance is the deficiency of P induced in the dry etching [13, 23]. While the annealing may recover the crystallinity lost during the dry etching [24], the high temperature treatment can even enhance the composition deficiency.

If the damaged layer is to be removed, a good selectivity between the damaged and undamaged parts is crucial. A method to remove the damaged part of InP is a wet etching using a 1% HF solution. This process removed the sidewall damage with a negligible change in the geometric dimension of the structure [25]. We have demonstrated a method to selectively remove the damaged part of the surface using a diluted HCl solution [13]. Undiluted HCl solutions etch InP. While the wet etching using HCl solutions is enhanced for the damaged surface of (In,Ga)As-InP quantum well structures, as-grown heterostructures as well as the InP substrates are not etched when the HCl solution is diluted to 3%. In this work, the samples were dipped in the solution for more than 3 h. It is emphasized that the exact duration of the etching is not crucial since the etching stops on its own when the damaged surface layer is no longer present.

For the ohmic contacts, a layer stack of Au/Ti/Ni/AuGe was evaporated on the contact areas. The layer thicknesses were 100, 50, 50, and 100 nm from the top (Au) to the bottom (AuGe). The contacts were alloyed at a temperature of 400 °C for 1 min under a flow of the N_2 gas. Note

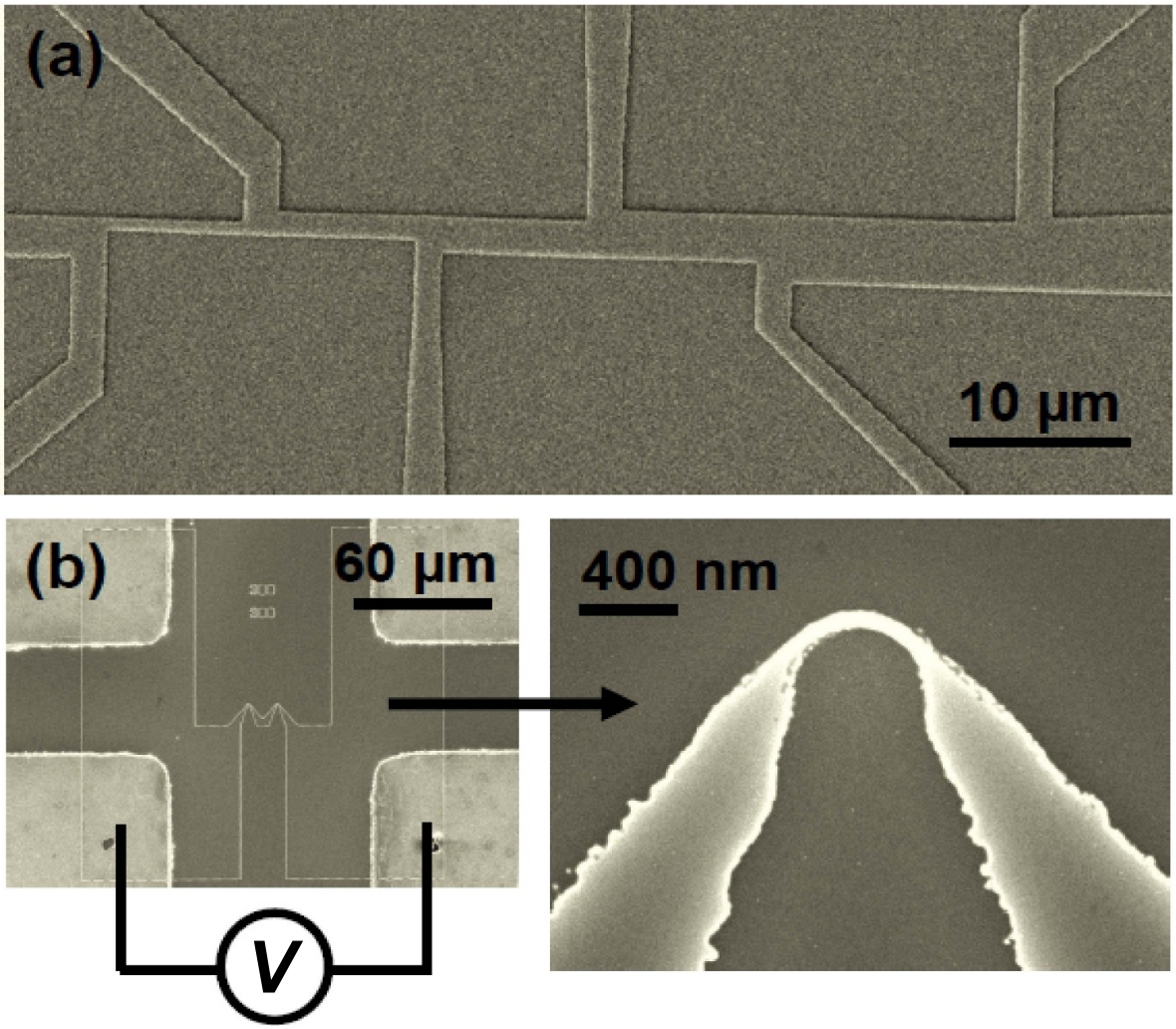

Figure 2. Scanning electron micrographs of mesa-etched (In,Ga)As-InP channels. An (In,Ga)As-InP heterostructure was processed using a reactive ion etching. The Hall-bar-type geometry in (a) was used to determine the width of the sidewall depletion. A rectification of *rf* excitations was demonstrated using the device geometry shown in (b). The voltage V was measured between the ohmic contacts attached to the narrow channel. Two hairpin channels are connected in series in this example. One of the hairpin channels is shown with an expanded scale.

that the Ti layer protected the Au layer from the alloying reaction that occurred between the Ni/AuGe layer and the heterostructure [26].

3. Transport properties

3.1. Sidewall depletion

We first confirm the almost complete absence of the lateral surface depletion for the narrow channels fabricated using the (In,Ga)As-InP heterostructure. In figure 3, we show inverse of the resistance R^{-1} of the channels normalized by the length L as a function of the channel width. The width was varied by employing the type of the device shown in figure 2(a). The scaling of the resistance with the channel size, which is manifested as the linear dependence, evidences that the surface conduction induced in the reactive ion etching was almost completely removed. By extrapolating the linear dependence to $L/R = 0$, the depletion width is extracted to be about zero at temperatures of both 4.2 and 300 K.

Using the sheet conductivity obtained from the slope together with the sheet electron density of $n_s = 6.6 \times 10^{15}$ m^{-2} determined by the Hall effect, the electron mobility in the etched channels was deduced to be 3.7 m^2 V^{-1} s^{-1}. The elastic mean free path $l_e = v_F\tau$ with v_F and τ being the Fermi velocity and the elastic scattering time, respectively, was estimated to be 0.5 μm. The length of the circular part of the hairpin channel shown in figure 2(b) is comparable with l_e. A considerable number of electrons are thus expected to travel ballistically along the circularly-shaped corner.

3.2. Magnetoresistance of narrow channels

Magnetotransport properties are expected to change qualitatively when the width W is varied since the transition between the regimes of $W > l_e$ and $W < l_e$ takes place for the channels.

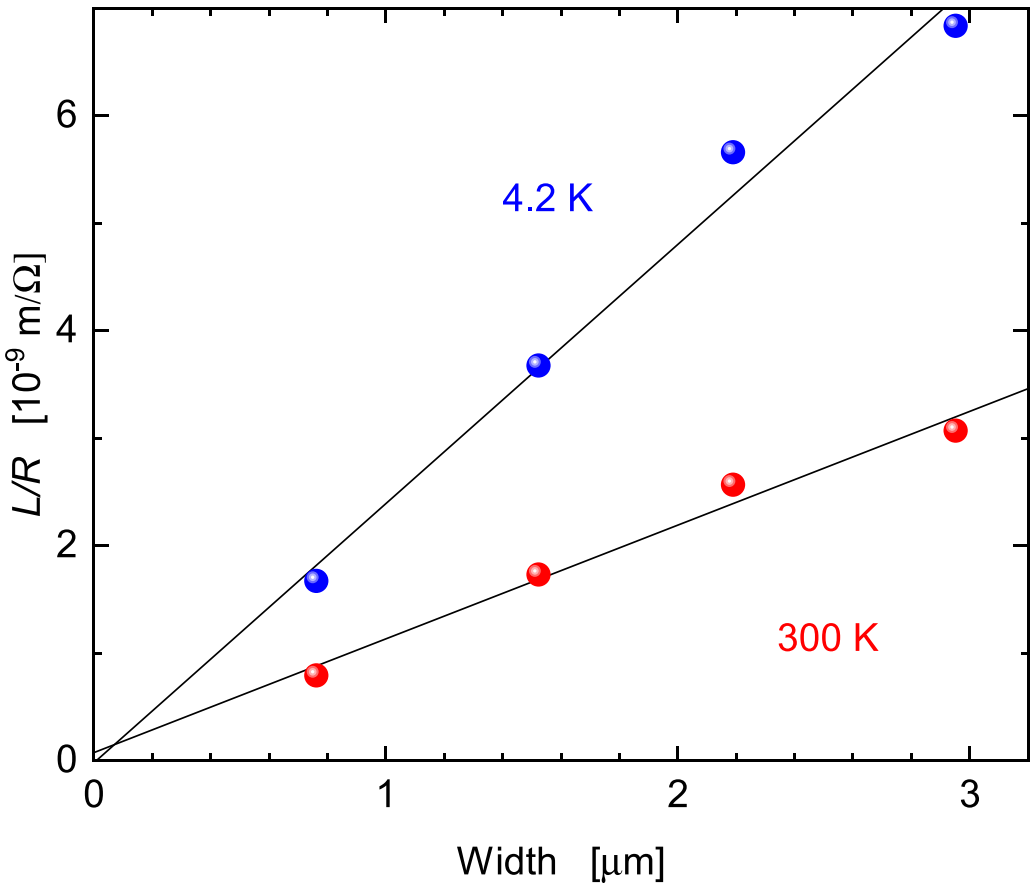

Figure 3. Estimation of sidewall depletion width for mesa-etched (In,Ga,A)-InP channels. The measurements were carried out in dark using a device similar to that shown in figure 2(a). The inverse of the resistance of the channels R^{-1} normalized by their length L is plotted as a function of the width of the channels. The linear dependencies shown by the solid lines indicate almost complete absence of the sidewall depletion at temperatures of both 4.2 and 300 K.

Figure 4 shows the variation of the magnetoresistance with W. For the wide channel ($W = 3.0\ \mu$m $> l_e$) shown in figure 4(a), the change of the resistance with the magnetic field is negligible until the Shubnikov-de Haas (SdH) oscillation emerges for $|B| > 2$ T. The magnetoresistance for narrow channels $W < l_e$ shown in figure 4(b) was obtained using the circularly-shaped devices, where the number N of the hairpin channels connected in series was 1 or 2. To be specific, each curve was obtained from a different device. The total resistance was divided by N to compare the resistance of a single hairpin channel. The overall increase of the resistance is a consequence of the reduction of W, i.e. the channel is narrower for the upper curve. The determination of the channel width was not simple due to the curved geometry. The resistance values at $B = 0$ are a representative of the width. The resistance at $B = 0$ additionally increased for narrow channels, giving rise to the negative magnetoresistance around $B = 0$. The negative magnetoresistance is attributed to the weak localization effect [27]. A negative magnetoresistance arises also for the constriction-like geometry from the fact that the number of occupied Landau levels is smaller in narrow channels than that for the bulk 2DEG due to the transverse confinement [28].

The resistance fluctuates irregularly with the change of the magnetic field for the narrow channels. The fluctuations are attributed primarily to the universal conductance fluctuations [29, 30] as the length of the narrow channel segment and l_e are comparable with each other, and so the diffusive contribution in the transport cannot be ignored. In addition, the geometrical meandering of the channel boundary, which is inevitable in real devices, causes random reflection for the electrons due to the absence of the sidewall depletion. The quantum interference in the randomly reflected ballistic trajectories gives also rise to the magnetoresistance fluctuations. The observation of the quantum fluctuations evidences that the phase coherence is maintained for the electrons in the channels. The curve in figure 4(c) shows the magnetoresistance obtained from a device where $N = 8$ hairpin channels were connected in series. The distance between the hairpin corners is larger than the phase coherence length. The suppression of the quantum fluctuations due to the averaging by the 8 independently fluctuating segments gave rise to the emergence of peaks indicated by the arrows. The peak reminds us of the effect of diffuse boundary scattering in long quasi-ballistic channels, for which $L > l_e > W$ [31, 32]. The diffuse component in the boundary

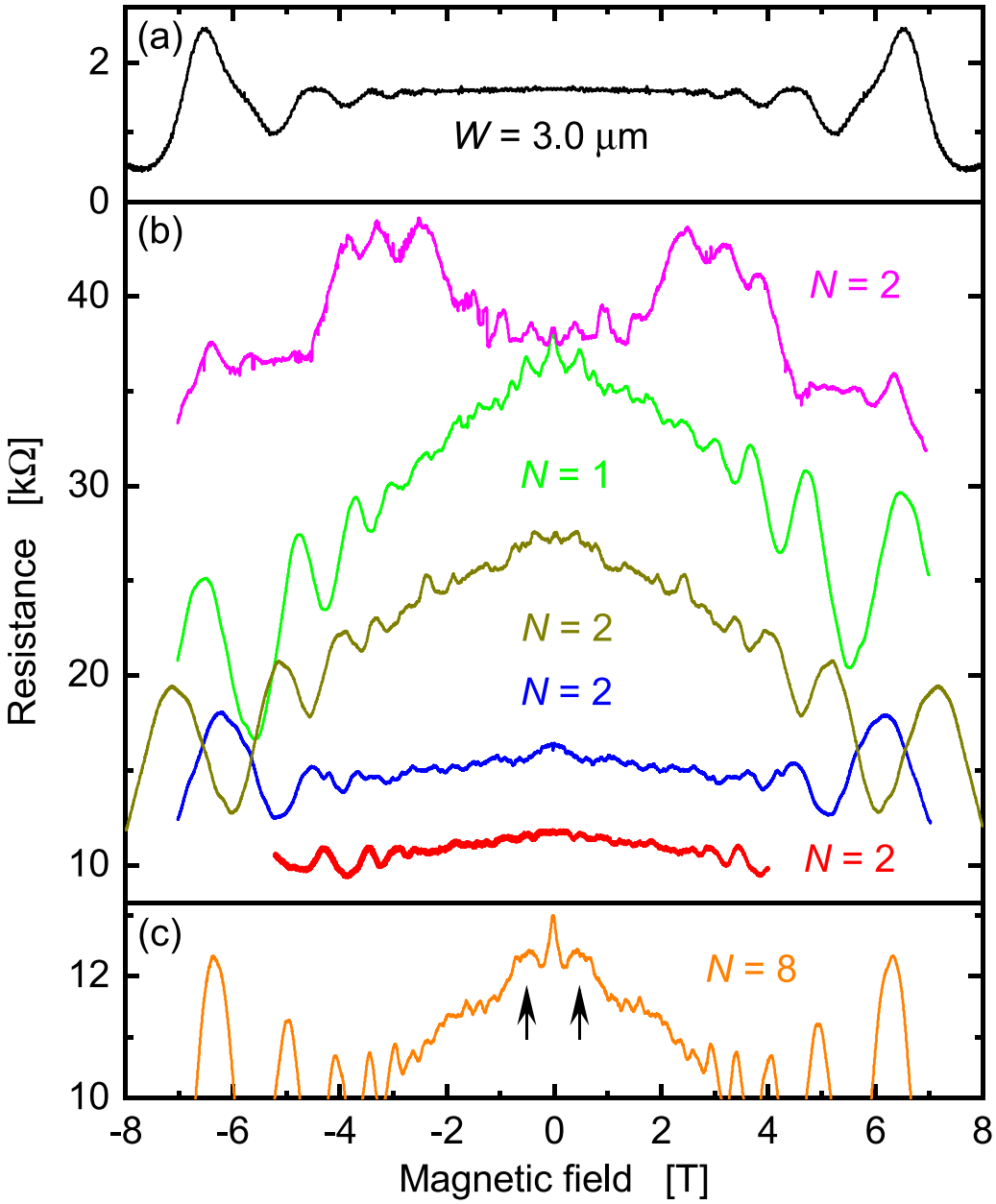

Figure 4. Variation of magnetoresistance with width of channels. The width W of the channel is 3.0 μm in (a). Narrow hairpin channels were employed in (b). The total resistance of the devices was divided by the number of the hairpin channels N. The curve in (c) was obtained from a sample having a series connection of $N = 8$ hairpin channels. The measurements were carried out at a temperature of 4.2 K.

scattering causes an increase of the resistance when the cyclotron diameter is comparable with the channel width. To be specific, the peak magnetic-field value $B_{\max}$ is related to W as [31]

$$W = 0.55\frac{\hbar k_{\mathrm{F}}}{eB_{\max}}, \tag{1}$$

where $k_{\mathrm{F}} = (2\pi n_s)^{1/2}$ is the Fermi wavenumber. The peak position in figure 4(c) corresponds to a width of 0.17 μm, which agrees with the width of 0.15 μm for the narrowest part of the circularly-shaped channels in this device.

3.3. Rectification of rf excitations by ballistic transport

For the hairpin devices shown in figure 2(b), the electron transport is not diffusive since the curved part of the channels is comparable with l_{e} in the length. We evidence in this subsection the existence of ballistic electrons with a demonstration of the rectification of *rf* voltages that emerges by tuning the strength of the magnetic field. In figure 5, we show the change of the voltage measured between the two ends of a channel when the magnetic field is varied. Note that two hairpin channels were connected in series in this device, similar to the one shown in figure 2(b). An *rf* excitation was applied to a nearby contact prepared on the Fe-doped InP substrate exposed by

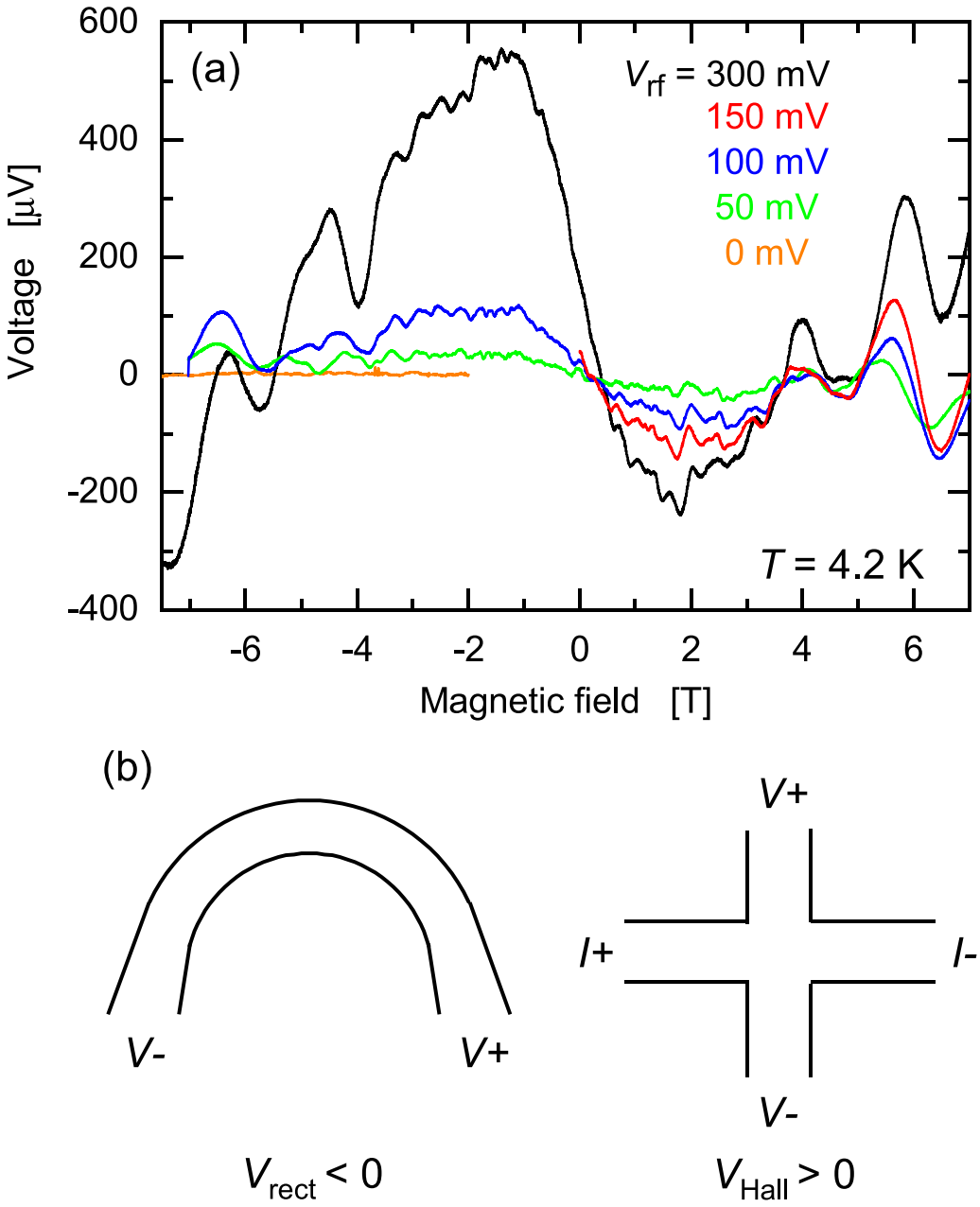

Figure 5. Magnetic-field-induced rectification of *rf* excitation. (a) The DC voltage was measured for a device with a series connection of two hairpin channels at a temperature of $T = 4.2$ K. The *rf* excitation with the amplitude V_{rf} at a frequency of 5.4 MHz was applied to the device by means of capacitive coupling. (b) For the magnetic field direction for which the Hall voltage V_{Hall} is positive for the configuration shown on the right-hand side, the rectified voltage V_{rect} becomes negative for the polarity defined on the left-hand side.

the dry etching. The electrical isolation of the excitation contact from the channel minimizes the possible influence of the DC offset of the *rf* generator on the voltage measurement. Moreover, the ground electrode of the *rf* generator was left unconnected to the device for the same reason. The electrons in the channel experienced the *rf* excitation through capacitive couplings. The actual excitation intensity was consequently orders of magnitude smaller than the nominal value [1]. Here, the cryostat employed for the low-temperature transport measurements worked as a cavity for the *rf* signals. The frequency of the *rf* voltage (5.4 MHz) was set to one of the resonance frequencies of the cavity. The excitation of the device was enhanced significantly in comparison to when an off-resonance frequency was used. That is, the cavity resonance partly compensated the reduction of the excitation intensity in the capacitive coupling.

The two-terminal voltage was about zero in the absence of the *rf* excitation, exhibiting primarily the Johnson noise. A finite DC voltage emerged, however, under the application of the *rf* excitation. Intensifying the excitation increased the magnitude of the voltage. The voltage was maximum at magnetic fields around ± 2 T, where the polarity of the voltage was antisymmetric with respect to the reversal of the magnetic field direction. The antisymmetric voltage manifests the

rectification effect resulting from the transmission asymmetry in the circular channel caused by ballistic electrons. The cyclotron radius of the 2DEG was $r_c = 75$ nm at the magnetic fields of ± 2 T, which is comparable to the curvature radius of the circular channel, see figure 2(b). The rectification is most efficient at the condition of $r_c = R$. The voltage hence decreased in amplitude when the magnetic field strengthened further as $|B| > 2$ T. On the other hand, the voltages for $|B| > 4$ T originated from the quantum Hall effect. The channel resistance becomes extremely large in the quantum Hall regime [33, 34], and so the *rf* excitation induces a large AC voltage in the channel. In principle, the induced AC voltage should be averaged out in the measurement of the DC voltage. However, real devices are not ideal. Asymmetric nonlinearities of the electrical properties originating from, for instance, nonideal ohmic contacts produced the nonzero DC voltage. The imperfection of the ohmic contacts becomes significant for the quantum Hall states due to the large resistivity developed by the 2DEG [33].

The DC voltages induced by the quantum Hall effect are not applicable for energy harvesting since they can be in either polarity contrary to the monopolar voltages produced by the rectification using the curved geometry. The output voltage does not increase when a large number of devices are connected in series in the quantum Hall regime. The voltages resulting from the circular geometry, in contrast, add up in the series connection [5]. For the strongest excitation of $V_{rf} = 0.3$ V in figure 5(a), the enhancement of the voltage at $B \sim -2$ T is considerably larger than that at $B \sim 2$ T. Given the large positive voltage at $B = 0$ in this case, the seeming asymmetric enhancement is attributed to the emergence of a magnetic-field-independent voltage offset for such a strong excitation.

The polarity of the rectification by the circular geometry depends on whether the carriers are electrons or holes, resembling the Hall effect. For the magnetic field direction that gives the positive slope of the Hall voltage ($V_{Hall} > 0$) in the measurement configuration shown on the right-hand side of figure 5(b), a voltage peak (dip) occurs at the negative (positive) magnetic field satisfying $r_c = R$ when the voltage is measured with the polarity illustrated on the left-hand side of figure 5(b).

The rectified voltage being zero in the absence of the *rf* excitation indicates that the device was not good enough to harvest energy from environmental electromagnetic noises due to the relatively low mobility of the 2DEG. Furthermore, the above manifestation of the ballistic transport has taken advantage of the fact that the *rf* excitation causes no difference for diffuse electrons apart from increasing the electron temperature. The voltage induced by the excitation cancels out for them since the transmission in the channel is symmetric regardless of the geometry. The excitation was intensified in figure 5(a) until the ballistic contribution became detectable.

The transmission asymmetry is produced by the partial backscattering associated with the non-specularity of the channel boundary. The rectification effect thus arises, in principle, when the condition $l_e \gg W$ is satisfied. Even if the circularly-shaped channel is longer than l_e, the rectification is accomplished within the sections of the channel having a length of $\sim l_e$. The dependence of the rectification efficiency on l_e in the quasi-ballistic transport regime consists of two parts. For a ballistic segment within the circularly-shaped channel having the length of l_e, the angle that the ballistic electrons are guided along the circle forming the channel is l_e/R. The rectification is more efficient when the electrons propagate ballistically over a larger angle. One may anticipate an exponential dependence of the rectification efficiency as $\exp(-cR/l_e)$ with c being a constant. The rectified voltage is then multiplied by the number of the ballistic segments. This improves the rectification effect in the situation that the transport is not fully ballistic. For a device in which N semicircle channels are connected in series, the total voltage is estimated to be $\propto N(\pi R/l_e)\exp(-cR/l_e)$.

3.4. Surface scattering

It is well-known that sidewall depletion is large for the mesa-etched channels fabricated from GaAs-(Al,Ga)As heterostructures [35]. The existence of the depletion layer actually has an advantage of working as a buffer to protect the 2DEG from the scatterers that may be induced at the surface by the attachment of foreign materials and/or by the defects generated in the etching. In this subsection, we show that such a scattering is inevitable for the channels fabricated from the (In,Ga)As-InP heterostructure due to the negligible surface depletion.

In figure 6, we compare the temperature dependence of the resistance for various widths of the channels. The hairpin channels were employed in the measurements, and so the larger resistance at RT indicates the width being narrower, similar to the situation in figure 4(b). For wide channels, the resistance decreases as temperature T is lowered with its approximate saturation for $T < 100$ K. The independence on T reflects the low-T saturation of μ that the bulk 2DEG exhibits due to the limit imposed by the alloy scattering. As the channels become narrower, the decrease of the resistance with lowering T is suppressed. The resistance eventually turns to increase at low temperatures, changing the curves to be U-shaped. The low-T increase of the resistance is attributed to the scattering of the 2DEG at the sidewalls of the channels given its enhancement for the narrower channels.

We have not identified the origin of the low-T increase of the resistance so far. For the intrinsic mechanisms of elastic electron scattering, the electron mobility should be almost independent of T at low temperatures. The kinetic energy of the electrons at the low T is fixed to be the Fermi energy for a degenerate system such as the 2DEG. The mobility when the phonon scattering is negligible thus exhibits no temperature dependence since the ratio between the kinetic energy and the strength of the scattering potentials associated with various disorders is unchanged. The temperature dependence is particularly weak for the (In,Ga)As-based quantum wells since the alloy scattering restricts μ to be relatively low to the degree that the phonon scattering plays no role at low T, see figure 1. The low-T increase of the resistance likely originates from an extrinsic environment effect. In cooling the samples from RT to 4.2 K in the cryostat, they were kept in a thin He atmosphere (1×10^4 Pa at RT) to enable heat transfer

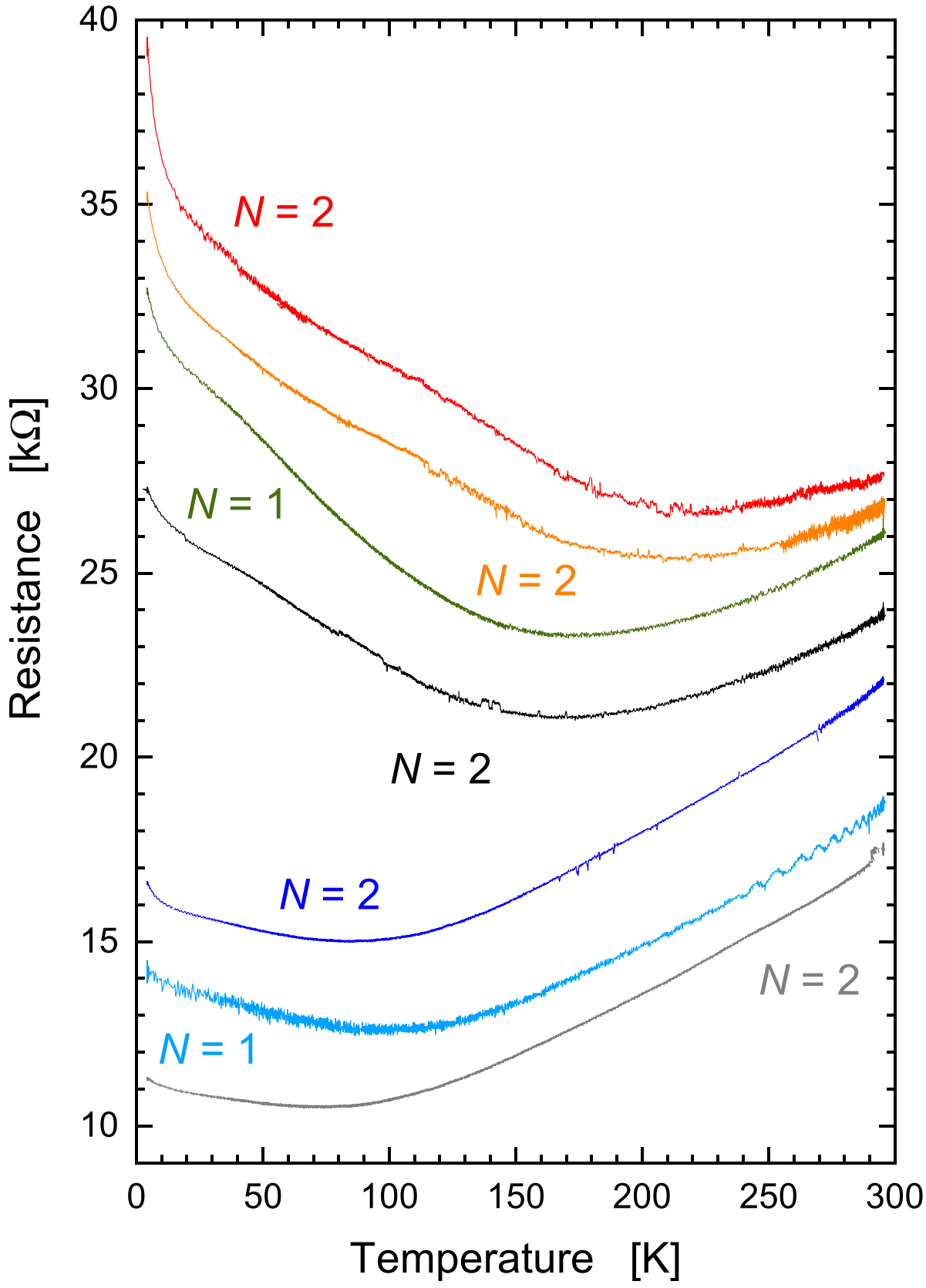

Figure 6. Comparison of temperature dependence of resistance for devices with various widths of channels. The total resistance has been divided by the number of hairpin channels *N*.

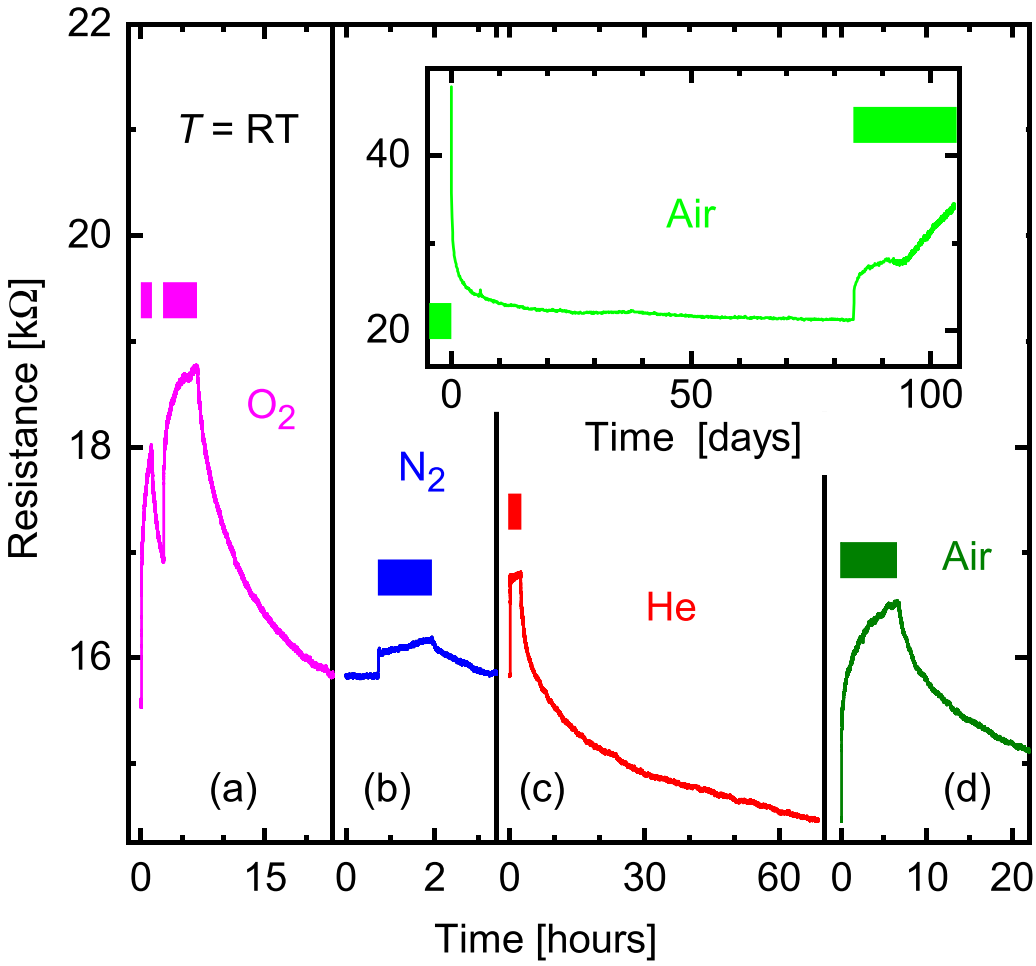

Figure 7. Time evolution of resistance in vacuum and under exposure to gases. The chamber in which the sample was kept was alternately being evacuated and filled with a gas. The increase and decrease of the resistance correspond to the exposure to the gas and evacuation, respectively. The gases were changed as O_2, N_2, He, and air. The rectangles indicate the periods of the gas exposure. For the case of the O_2 gas, the sample chamber was temporarily evacuated in the middle of the exposure to the gas. The measurements were carried out at room temperature. The device consisted of eight hairpin channels connected in series. For the curve shown in the inset, the sample kept initially in air was placed in vacuum and then exposed to air again.

from the samples to the liquid He bath. More He atoms will be adsorbed at the surface of the channels as the temperature decreases. This will result in increasing the number of surface scatterers for lower T. We show below that the attachment of He atoms at the channel surface indeed causes scattering for the 2DEG. It needs to be pointed out, however, whether the He atoms in the heat-exchange gas were responsible for the low-T increase of the resistance is unclear, as will be discussed later.

We demonstrate the extrinsic surface scattering in figure 7. The time evolution of the resistance of a narrow channel was measured at RT while the chamber in which the sample was kept was either in vacuum or filled with a gas. Following the initial state of the chamber being evacuated by a vacuum pump, a gas was introduced to the chamber with the atmospheric pressure. This measurement procedure was repeated while the gas was varied as O_2, N_2, He and air. In all the cases, the resistance increased during the exposure to a gas. For the case of the O_2 gas in figure 7(a), the sample chamber was temporarily evacuated in the middle of the exposure to the gas and then refilled with the O_2 gas. The time evolution of the resistance is seen to be unaffected qualitatively by the initial coverage of the O_2 molecules on the surface.

Interestingly, the manner the resistance increased depended on the gas species. The resistance change was large for the O_2 gas, whereas the N_2 gas caused a small change. The change was of an intermediate degree for the He gas. In the exposure to the air, the resistance increase was larger than one may anticipate given the fractions of O_2 and N_2 in the air being 21 and 78%, respectively. The wetting of the channel surface by moisture is thus indicated to cause, at least, a considerable scattering.

The decrease of the resistance when the gas was removed from the chamber was slower than the increase. That is, the desorption of the gas molecules was slower than their attachment. The complete removal of the gas molecules from the surface takes apparently a very long time. One finds in figure 7(c) that the resistance did not reach a saturation even after the evacuation for 3 days. In the inset of figure 7, the gradual saturation of the resistance when a sample was kept in vacuum over

nearly 3 months is shown with the behavior of the resistance increase when air was introduced into the sample chamber.

It is suggested that there are two styles in the manner the molecules are attached to the surface. For the cases of the N_2 and He gases, a rapid initial increase was followed by a slow nearly-linear increase of the resistance. Such a two-step process was not observed for the O_2 gas and air, where the resistance increase slowed down gradually.

The molecules attached to the surface induce charges through a charge transfer with the semiconductors. The molecules may be already charged before their attachment. The resultant random distribution of surface charges acts as scatterers for the 2DEG. The large and small changes of the resistance for the cases of the O_2 and N_2 gases, respectively, presumably reflect the electronegativity of the involved materials, i.e. whether electrons are given to or extracted from the surface. Obviously, the resistance is altered by positive and negative charges differently, while the (In,Ga)As conduction channel was of *n*-type.

The gas molecules adsorbed at the top surface of the (In,Ga)As-InP heterostructure are not relevant for the resistance change since the InP barrier layer separates the scatterers to be away from the 2DEG. Although the scattering for the 2DEG is caused only by the molecules attached to the side surface of the mesa-etched channels, the channel resistance responds sensitively. The high sensitivity is enabled by the quasi-ballistic conduction $l_e \gg W$. The surface scattering effectively reduces l_e to $\sim W$, and so the effect on the resistance is considerable. The surface scattering, therefore, becomes more crucial for narrower channels.

The localized scattering at the side surface implies that the surface scattering can be, in fact, helpful for the rectification effect. The cyclotron orbit that fits within the curved channel at the magnetic field satisfying $r_c = R$ is unaffected by the surface scattering since the electron does not collide with the channel boundary. The surface scattering, on the other hand, enhances the backscattering for the electrons moving in the opposite direction. The transmission asymmetry due to the curved geometry will consequently increase. If this is indeed the case, the rectification effect is expected to be the strongest at the lowest temperature even when the temperature dependence of the resistance is U-shaped, where the nominal value of l_e is the largest at the bottom temperature of the U-shaped curve. The Thomas-Fermi screening length of a two-dimensional system is independent of the carrier density and is $\lambda_{TF} = 2\pi\varepsilon_0\varepsilon_r\hbar^2/e^2m^* = 12$ nm for $In_{0.75}Ga_{0.25}As$. Here, $\varepsilon_r = 14.4$ is the dielectric constant and m^* is the effective mass. It is plausible that the electrons in the interior of the channel are not affected significantly by the surface scatterers due to the screening.

While the effect of the surface scattering is compared among the samples having various widths in figure 6, a comparison of the temperature dependence is made in figure 8 for one narrow-channel sample when the number of the surface scatterers was changed. Here, the sample was kept in air or in vacuum prior to the measurements to alter the number of the molecules attached to the surface. It is noted that the sample was in the thin He atmosphere during the measurements to enable cooling. The sample was cooled from RT to 4.2 K in less than an hour to minimize the effects resulting from the surface adsorption of the He gas. As one would expect, even the resistance at RT is recognized to increase when the surface scattering is strong. At high temperatures, the difference of the resistance induced by keeping the sample in air or vacuum is almost independent of temperature, i.e. the surface scattering imposes an offset in this regime. As shown by the green curve, the degree of the surface scattering changes continuously depending on how long the sample was kept in vacuum prior to the measurements.

The low-T increase of the resistance is enhanced by the exposure to the air. The surface scattering is thus found to be responsible for the anomalous low-T behavior. On the other hand, the adsorption of the He atoms from the thin atmosphere at low T does not appear to be the origin for the anomalous behavior. The low-T increase was caused by the molecules attached to the surface in the exposure to the air. One may need to take the surface migration of the adsorbed molecules and its low-T freezing into consideration for understanding the anomalous behavior.

In figure 8, the sample cooling was carried out in dark. The sample was then illuminated when the temperature reached 4.2 K. The illumination reduced the resistance of the channel significantly, where the photoconduction effect was found to be persistent. After the illumination had been turned off, the sample was warmed up to RT in the darkness. Despite the large resistance change, the concentration of the 2DEG increased merely about 10% after the illumination according to the SdH oscillation (not shown). The photoconduction is thus indicated to have occurred to a large extent as a parallel conduction in the undoped InP layers that sandwiched the (In,Ga)As quantum-well layer. The resistance became nearly the same after the illumination independent of the attachment of the molecules at the surface. When the temperature was raised to RT and the persistent photoconduction consequently vanished, the resistance returned to the initial values before the measurement cycles, i.e. the resistance at RT remained to be influenced by the surface scattering with the same strengths. The illumination thus did not remove the gas molecules and the moisture in the air attached to the surface. The disappearance of the effect of the surface scattering after the illumination at low T indicates that the surface scattering plays no role for the carriers generated in the barrier layers by the photo excitation. The electrical conduction properties were apparently almost completely dominated by the parallel conduction carriers instead of the 2DEG. The electrons in the barrier layers have a low mobility, and so the transport properties of these diffusive electrons are little changed by the surface scattering. The high mobility of the 2DEG in the (In,Ga)As quantum well is manifested to be crucial for the high sensitivity to the surface scattering.

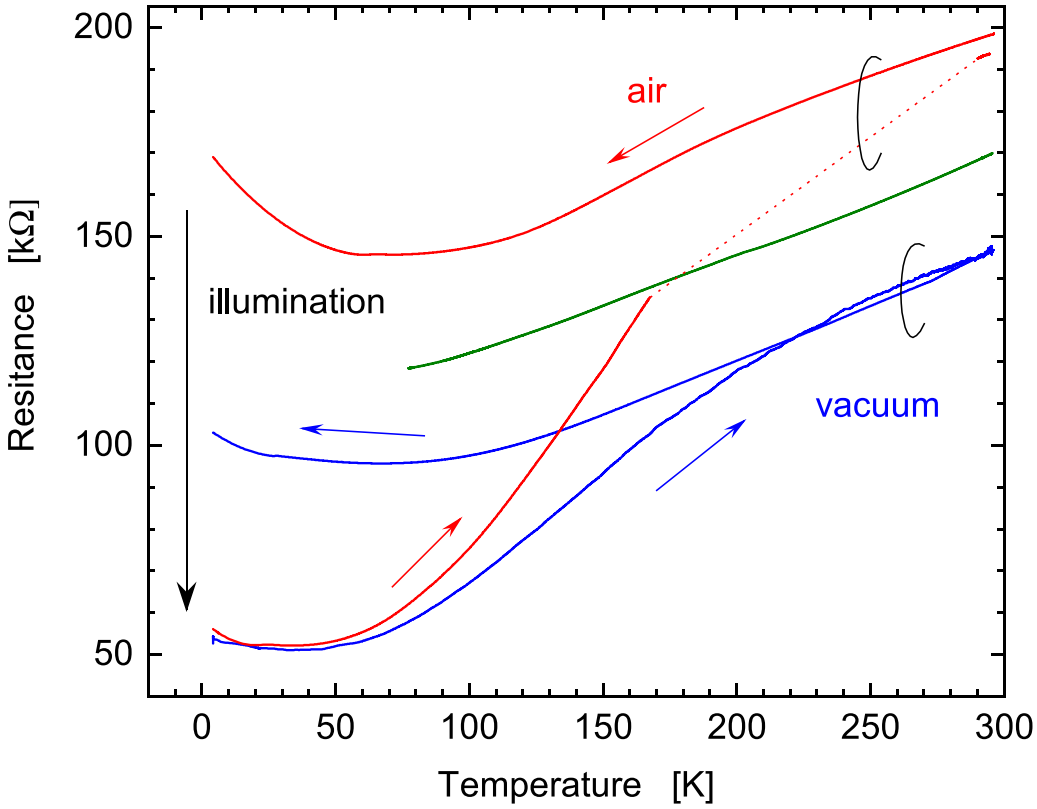

Figure 8. Effects of air exposure and illumination. The resistance was obtained from a sample in which 8 hairpin channels were connected in series. The sample was kept in air and in vacuum at RT prior to the measurements for the red and blue curves, respectively. For these curves, the sample was cooled in dark, illuminated at 4.2 K, and warmed to RT without the illumination. The temperature dependence in the cooling procedure is also shown for a case where the sample was kept in vacuum briefly prior to the measurement as the green curve. In all the cases, the sample chamber was filled with a thin He gas (1×10^4 Pa at RT) during the measurements.

4. Conclusions

A magnetic-field-induced rectification of *rf* voltages has been demonstrated using circularly-shaped 2DEG channels fabricated from an (In,Ga)As-InP heterostructure. The successful device operation evidences the ballistic transport of electrons for the small channel sizes enabled by the absence of the surface depletion for the In-rich quantum well. The size reduction relied on the smoothness of the etched surface accomplished by a reaction ion etching. The negligible surface depletion, on the other hand, means the lack of protection for the 2DEG, where the surface scattering has been shown to increase the resistance of narrow channels. The degree of the resistance increase depends on the gas species, and so the effect may be utilized for a gas sensing. While a persistent photoconduction has been shown to take place at low temperatures, the photocarriers contributed to the transport properties primarily as a parallel conduction in the undoped InP barrier layers.

Data availability statement

The data cannot be made publicly available upon publication because no suitable repository exists for hosting data in this field of study. The data that support the findings of this study are available upon reasonable request from the authors.

ORCID iDs

A Aleksandrova https://orcid.org/0000-0001-6588-153X
Christian Golz https://orcid.org/0000-0001-6839-3611
Mykhaylo Semtsiv https://orcid.org/0000-0003-4007-3282
Y Takagaki https://orcid.org/0000-0002-6691-1005

References

[1] Hortelano V, Weidlich H, Masselink W T, Mahler G and Takagaki Y 2017 Demonstration of magnetic-field-induced rectification using circular ballistic channels with a rough boundary *Semicond. Sci. Technol.* **32** 125005
[2] Weidlich H 2015 Vorrichtung zur Führung von Ladungsträgern und deren Verwendung *European Patent Application* 15000040.4
[3] Sánchez D and Büttiker M 2004 Magnetic-field asymmetry of nonlinear mesoscopic transport *Phys. Rev. Lett.* **93** 106802
[4] Sánchez D and Kang K 2008 Validity and breakdown of onsager symmetry in mesoscopic conductors interacting with environments *Phys. Rev. Lett.* **100** 036806
[5] Hortelano V, Weidlich H, Masselink W T and Takagaki Y 2019 Magnetic-field-induced transport asymmetry in two-terminal circular ballistic bends *J. Appl. Phys.* **125** 145301
[6] Iwata J, Ida J, Futura T, Noguchi K and Itoh K 2016 Confirmation of high efficiency on rectenna with high

impedance antenna and optimized gate controlled diode for RF energy harvesting *IEEE Sensors* vol 2016 pp 1–3
[7] Mori T, Ida J, Momose S, Itoh K, Ishinashi K and Arai Y 2018 Diode characteristics of a super-steep subthreshold slope PN-body tied SOI-FET for energy harvesting application *J. Electron Dev. Soc.* **6** 565–70
[8] Ida J 2022 Ultra low power electronics using PN-body tied SOI-FET *Oyo Buturi* **91** 144–50
[9] Hemour S , Zhao Y, Lorenz C H P, Houssameddine D, Gui Y, Hu C-M and Wu K 2014 Towards low-power high-efficiency RF and microwave energy harvesting *IEEE Trans. Microw. Theory Tech.* **62** 965–76
[10] Hemour S and Wu K 2014 Radio-frequency rectifier for electromagnetic energy harvesting: development path and future outlook *Proc. IEEE* **102** 1667–91
[11] Akinaga H 2020 Recent advances and future prospects in energy harvesting technologies *Jpn. J. Appl. Phys.* **59** 110201
[12] Zulkepli N, Yunas J, Nohamed M A and Hamzah A A 2021 Review of thermoelectric generators at low operating temperatures: working principles and materials *Micromachines* **12** 734
[13] Hortelano V, Weidlich H, Semtsiv M P, Masselink W T, Ramsteiner M, Jahn U, Biermann K and Takagaki Y 2018 Nanostructuring of conduction channels in (In,Ga)As-InP heterostructures: overcoming carrier generation caused by Ar ion milling *Appl. Phys. Lett.* **112** 151602
[14] Wada O 1984 Ar ion-beam etching characteristics and damage production in InP *J. Phys. D: Appl. Phys.* **17** 2429–37
[15] Soshnikov I P, Lunev A V, Gaevskii M E, Nesterov S I, Kulagina M M, Rotkina L G, Barchenko V T, Kalmykova I P, Efimov A A and Gorbenko O M 2001 The formation of developed morphology on the indium phosphide surface by ion argon beam sputtering *Tech. Phys.* **46** 892
[16] Bouadma N, Devoldere P, Jusserand B and Ossart P 1986 Ion beam etching and surface characterization of indium phospide *Appl. Phys. Lett.* **48** 1285–87
[17] Kosior L, Radziewicz D, Zbrowska-Lindert I, Stafiniak A, Badura M and Sciana B 2016 Epitaxial regrowth of InP/InGa As heterostructure on patterned, nonplanar substrates *Mater. Sci.-Poland* **34** 872–80
[18] Galeuchet Y D, Roentgen P and Graf V 1988 Buried GaInAs/InP layers grown on nonplanar substrates by one-step low-pressure metalorganic vapor phase epitaxy *Appl. Phys. Lett.* **53** 2638–40
[19] Deng L 2013 Dry etching of InP-based materials using a high-density ICP plasma system *Semicond. Today* **7** 82–87
[20] Sivak N P, Fan X Z and Ghodssi R 2015 Fabrication challenges for indium phosphide microsystems *J. Micromech. Microeng.* **25** 043001
[21] (Available at: www.hhi.fraunhofer.de/en/departments/pc/research-groups/processing.html)
[22] Cullis A G and Hutchison J L 2001 Microscopy of semiconducting materials *Proc. Royal Microscopical Soc. Conf.* pp 25–29
[23] Katzschner W, Steckenborn A, Loeffler R and Grote N 1984 Ion beam milling of InP with an Ar/O_2-gas mixture *Appl. Phys. Lett.* **44** 352–54
[24] Hirano R and Kanazawa T 1990 Heat treatments of InP wafers *J. Cryst. Growth* **106** 531–36
[25] Bottner T, Krautle H, Kuphal E, Miethe K and Hartnagel H L 1996 *8th Int Conf. Indium Phosphide and Related Mater.* pp 115–18
[26] Morais J, Fazan T A, Landers R and Sato E A S 1996 Ohmic contact formation on *n*-InP *J. Appl. Phys.* **79** 7058–61
[27] Bergmann G 1984 Weak localization in thin films *Phys. Rep.* **107** 1–58
[28] van Houten H, Beenakker C W J, van Loosdrecht P H M, Thornton T J, Ahmed H, Pepper M, Foxon C T and Harris J J 1988 Four-terminal magnetoresistance of a two-dimensional electron-gas constriction in the ballistic regime *Phys. Rev.* **37** 8534–36
[29] Lee P A, Stone A D and Fukuyama H 1987 Universal conductance fluctuations in metals: effects of finite temperature, interactions and magnetic field *Phys. Rev.* B **35** 1039–70
[30] Beenakker C W J and van Houten H 1988 Flux-cancellation effect on narrow-channel magnetoresistance fluctuations *Phys. Rev.* B **37** 6544–46
[31] Thornton T J, Roukes M L, Scherer A and van de Gaag B P 1989 Boundary scattering in quantum wires *Phys. Rev. Lett.* **63** 2128–31
[32] Wu B-Y *et al* 2020 A self-assembled graphene ribbon device on SiC *ACS Appl. Electr. Mater.* **2** 204–12
[33] Wixforth A, Scriba J, Wassermeier M, Kotthaus J P, Weimann G and Schlapp W 1989 Surface acoustic waves on GaAs/$Al_xGa_{1-x}As$ heterostructures *Phys. Rev.* B **40** 7874–87
[34] Esslinger A, Winkler R W, Rocke C, Wixforth A, Kotthaus J P, Nickel H, Schlapp W and Lösch R 1994 Ultrasonic approach to the integer and fractional quantum hall effect *Surf. Sci.* **305** 83–86
[35] Takagaki Y, Kosugi T, Gamo K, Namba S and Murase K 1990 Effect of low temperature photoconduction on the depletion width in GaAs-AlGaAs wire *Semicond. Sci. Technol.* **5** 634–37